Bridge Foundation Scour

Jean-Louis BRIAUD [1] and Seung Jae OH[2]
[1] *President of ISSMGE and Professor, Dept. of Civil Engineering, Texas A&M Univ., College Station, Texas, USA*
[2] *Ph.D., Research Assistant, Dept. of Civil Engineering, TEXAS A&M Univ., College Station, Texas, USA*
E-mail: jlbriaud@civil.tamu.edu

1. EROSION PROCESS

1.1 Soil erosion

Three things happen when the water starts flowing. First, a drag force and associated shear stresses develop at the interface between the soil particle and the water flowing over it. Second, the normal stress on top of the soil particle decreases because of the water flow. Indeed, as the velocity increases around the particle or the obstacle, the pressure drops to maintain conservation of energy according to Bernoulli's principle. This phenomenon is similar to the air flow on top of an airplane wing where the pressure is lower than below the wing thereby developing the uplift force necessary for the plane to fly. Third, the normal stresses and shear stresses applied at the boundaries are fluctuating with time because of the turbulence in the water. These fluctuations find their roots in the appearance and disappearance of eddies, vortices, ejections and sweeps in the flowing water; and they can contribute significantly to the erosion process especially at higher velocities. In some cases they are the main reason of erosion.

1.2 Rock erosion

Rock erodes through two main processes: rock substance erosion and rock mass erosion. Rock substance erosion refers to the erosion of the rock material itself while rock mass erosion refers to the removal of rock blocks from the jointed rock mass. Rock substance erosion includes three sub-mechanisms: erosion due to the hydraulic shear stress created by the water at the rock-water interface, erosion due to abrasion caused by sediments rubbing against the rock during the flow, and impact of air bubbles that pit the rock surface due to cavitation at very high velocities. Rock mass erosion includes two sub mechanisms: erosion due to slaking, and erosion due to block removal between joints. Slaking can occur when a rock, such as a high plasticity shale in an ephemeral stream, dries out and cracks during summer months; these small blocks are then removed by the next big flood. Block removal can occur if, during high turbulence events, the difference in pressure between the top and the bottom of a rock block becomes large enough to overcome the weight and side friction on the block.

2. TESTING FOR ERODIBILITY

An apparatus measuring the erosion function was developed in the early 1990s, called the EFA (Erosion Function Apparatus) (Fig. 1, Briaud et al., 2001). The principle is to go to the site where erosion is being investigated, collect samples within the depth of concern, bring them back to the laboratory, and test them in the EFA. The 75 mm outside diameter sampling tube is placed through the bottom of the conduit where water flows at a constant velocity. The soil or rock is pushed out of the sampling tube only as fast as it is eroded by the water flowing over it. For each velocity, an erosion rate is measured and a shear stress is calculated using Moody's chart (Moody, 1944). Point by point the erosion function is obtained.

For fine grained and coarse grained soils, ASTM standard thin wall steel tube samples are favoured. If such samples cannot be obtained (e.g.: coarse grained soils), Split Spoon SPT samples are obtained and the coarse grained soil is reconstituted in the thin wall steel tube. Fortunately in the case of erosion of coarse grained soils, soil disturbance does not affect the results significantly. If it is representative of the rock erosion process to test a 75 mm diameter rock sample, the rock core is placed in the thin wall steel tube and tested in the EFA. The rate of erosion can be very different for different soils.

While the EFA provides an accurate method for determining the erosion resistance of soils in a laboratory setting, there is still a need for a simple method and device that can be used in the field. The Pocket Erodometer Test (PET) is a simple test which can be performed in a few seconds with an inexpensive, compact, and very light instrument. The Pocket Erodometer is a regulated mini jet impulse generating device (Fig.2). The jet is aimed horizontally at the vertical face of the soil sample. The depth of the hole (mm) in the surface of the sample created by 20 impulses of water is recorded. The hole depth is compared with an erosion chart to determine the erodibility category of the soil. This erosion category allows the engineer to make preliminary decisions in erosion related work. The development of the device is ongoing, but early results show that this very simple tool can provide relatively accurate results when calibrated with the EFA.

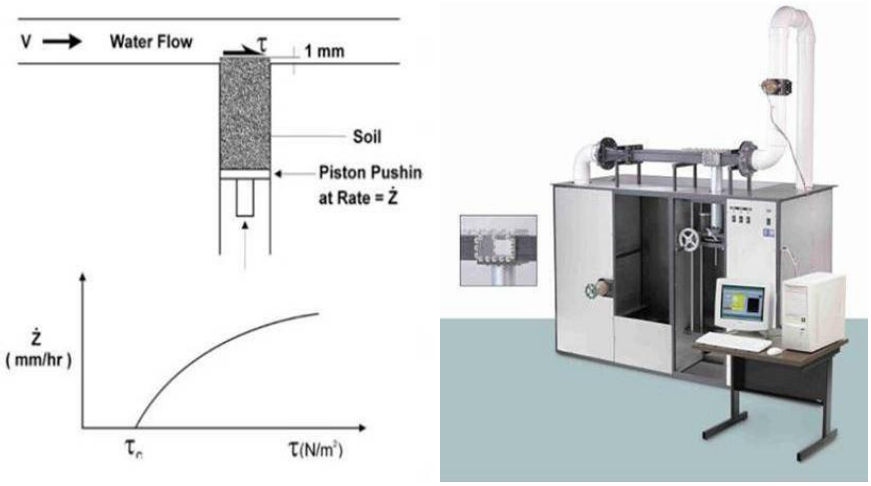

Figure 1 Erosion Function Apparatus to measure erodibility (Briaud et al., 1999).

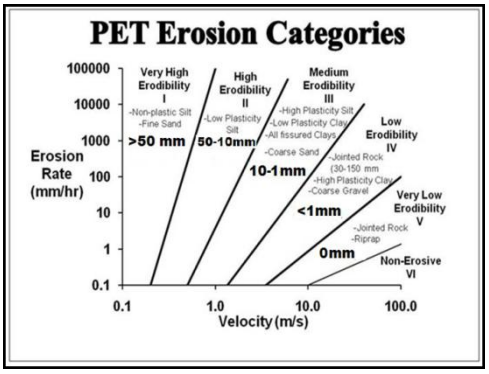

Figure 2 Pocket Erodometer and PET erosion category chart.

3. EROSION CLASSIFICATION

Categories are used in many fields of engineering: soil classification categories, hurricane strength categories, earthquake magnitude categories. Such categories have the advantage of quoting one number to represent a more complex condition. Erosion categories are proposed (Fig. 3) in order to bring erodibility down in complexity from an erosion rate vs shear stress function to a category number. Such a classification system can be presented in terms of velocity (Fig. 3) or shear stress (Fig. 4).

The erosion categories are proposed on the basis of 15 years of erosion testing experience. In order to classify a soil or rock, the erosion function is plotted on the category chart and the erodibility category number for the material tested is the number for the zone in which the erosion function fits. Note that using the water velocity is less representative and leads to more uncertainties than using the shear stress; indeed the velocity and the shear stress are not linked by a constant. Nevertheless the velocity chart is presented because it is easier to gage a problem in terms of velocity.

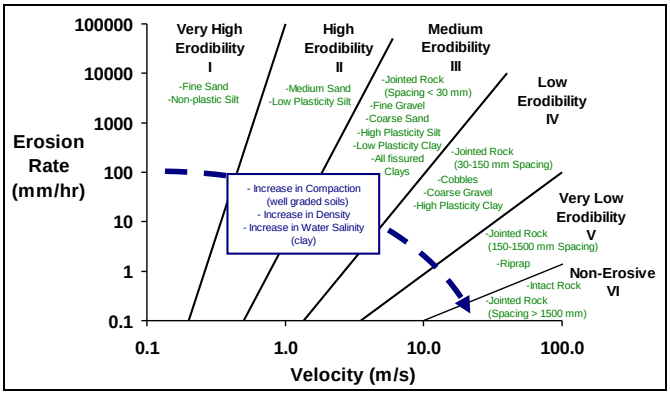

Figure 3 Proposed erosion categories for soils and rocks based on velocity (Briaud, 2008).

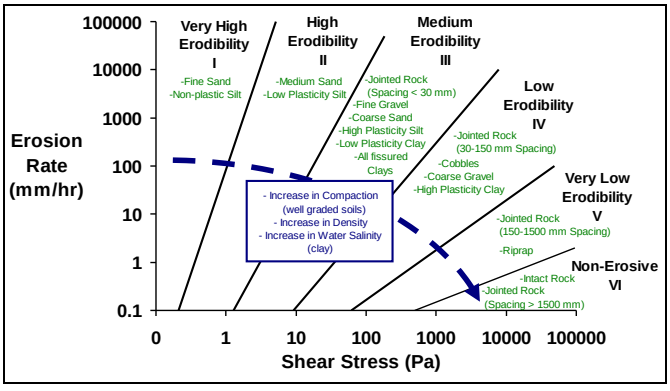

Figure 4 Proposed erosion categories for soils and rocks based on shear stress (Briaud, 2008).

4. BRIDGE SCOUR PREDICTION

Most prediction equations to estimate bridge scour depths have been developed on the basis of laboratory flume test results using cohesionless soil. Unfortunately these same equations are also used for cohesive soil which have much lower erosion rate than cohesionless soil. It usually takes less than a day for cohesionless soil to reach the maximum scour depth around a bridge support under a constant flow rate but for a cohesive soil the scour depth developed in a day maybe a small percent of the maximum scour depth because of the slower erosion rate. Studies of bridge scour depths in cohesive soils with consideration of soil erodibility and time dependence have been performed at Texas A&M University since 1990.

5. SCOUR TYPES

Bridge scour is the aggradation or degradation of the riverbed around the bridge structure, and it is usually divided into general scour, contraction scour and local scour.

General scour happens without the existence of a bridge. One example of general scour is the case of the artificial straightening of a channel in a river which increases the flow velocity in the river and leads to erosion. Contraction scour results from the acceleration of the flow due to the constriction of a channel by the approach embankments. Local scour happens due to the velocity increase and turbulence around bridge obstacles such as piers and abutments. The definition of contraction scour and local scour is shown in Fig. 5. Fig. 6 illustrates that the maximum contraction scour (Fig. 6 a) occurs where the velocity is the highest (Fig. 6 b) while the maximum abutment scour (Fig. a) occurs where the turbulence intensity is the highest (Fig. c).

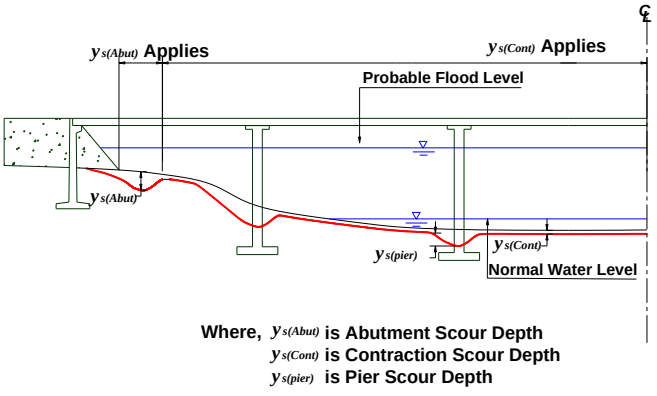

Figure 5 Definition of contraction and local bridge scour.

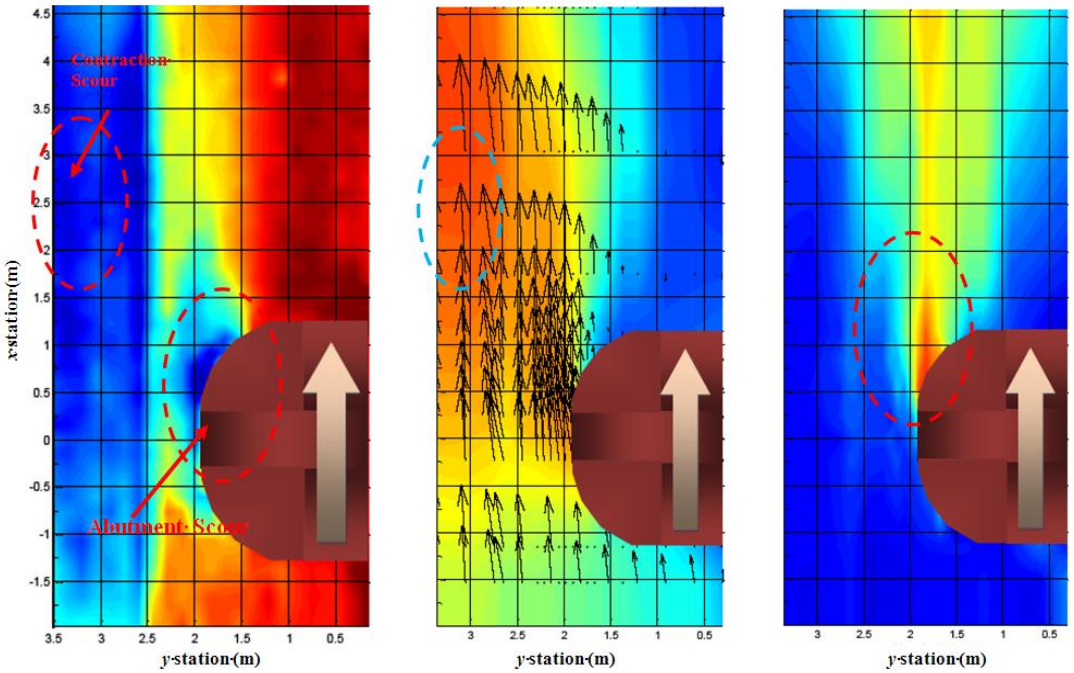

(a) Scour pattern after 320 hours (b) Initial surface velocity (c) Initial turbulence intensity

Figure 6 Comparison of scour pattern and velocity pattern (Oh, 2009).

6. MAXIMUM PIER SCOUR

A method to predict the maximum pier scour depth in cohesive soil was proposed by Gudavalli (1997) after conducting experimental research on pier scour using circular piers in deep water condition ($y_1 / a \geq 1.43$ where y_1 is the approach water depth and a is the pier diameter). He used 2 types of sand and 3 types of clay during his experiments, and proposed Eq. (1). Li (2002) studied complex pier scour considering the shallow water effect, pier shape effect, attack angle effect and group pier effect, and then proposed Eq. (2).

$$y_{s(Pier)}(mm) = 0.18\left(\frac{aV}{v}\right)^{0.635} \quad (1)$$

$$y_{s(Pier)}(mm) = 0.18 \cdot K_w \cdot K_{sp} \cdot \left(\frac{a'V}{v}\right)^{0.635} \quad (2)$$

where $y_{s(Pier)}$ is the maximum pier scour depth, a is the width of the pier, a' is the projected pier width perpendicular to the flow for rectangular pier, L is the length of the pier, is the angle of attack, V is the mean velocity at the location of the pier if the pier was not there, v is kinematic viscosity of water (10^{-6} m^2/s at 20 ℃),K_w is the correction factor of water depth effect, and K_{sp} is the correction factor of pier spacing effect.

Although 5 types of soil were used in these projects, the soil properties were not included in 1997 and 2002 equations. New data analyses were conducted in 2009 and a new methodology was developed which including a soil property. The analyses started with a dimensional analysis.

6.1 Dimensional analysis

The parameters influencing pier scour can be listed as:

$$y_{s(Pier)} = f(a, L, y_1, \theta, g, V_1, V_c, S, sh) \quad (3)$$

where S is the spacing between two piers (measured center to center), sh is the shape of the pier nose and $V_c = \sqrt{\frac{\tau_c \cdot y_1^{1/3}}{\rho \cdot g \cdot n^2}}$ is the critical velocity of the soil, τ_c is the critical shear stress of the soil, n is Manning's coefficient, g is gravitational acceleration, ρ is unit mass of water, y_1 is the approach water depth, V_1 is the mean velocity at the location of the pier if the pier was not there

Eq. (3) can be normalized through dimensional analysis and becomes:

$$\frac{y_{s(Pier)}}{a} = f\left(\frac{L}{a}, \frac{y_1}{a}, \theta, Fr_{(pier)}, Fr_{c(pier)}, \frac{S}{a}, sh\right) \quad (4)$$

where $Fr_{(pier)}\left(=\frac{V_1}{\sqrt{g \cdot a}}\right)$ is Froude number based on approach velocity and pier width, and $Fr_{c(pier)}\left(=\frac{V_c}{\sqrt{g \cdot a}}\right)$ is the critical Froude number based on critical velocity and pier width

Since pier scour develops until the shear stress acting around the pier equals to the critical shear stress, therefore the maximum pier sc our equation can be expressed as:

$$\frac{y_{s(Pier)}}{a} = K_1 \cdot K_2 \cdot K_L \cdot K_w \cdot K_{sp} \cdot \alpha_1\left(\beta_1 \cdot Fr_{(pier)} - Fr_{c(pier)}\right)^{\chi_1} \quad (5)$$

where K_1 is correction factor of pier shape, K_2 is the correction factor of attack angle, K_L is the correction factor of the aspect ratio

of a rectangular pier, K_w is the correction factor of the water depth effect, K_{sp} is the correction factor of pier spacing, α_1, β_1 and χ_1 are constant. Note that the amplification factor β_1 (>1) is necessary to include the magnification effect of the turbulence around the pier

6.2 Single circular pier in deep water

Data for single circular piers in deep water condition Gudavalli (1997) and Li (2002) were collected and re-analyzed to develop a new pier scour equation. For a single circular pier in deep water, Eq. (5) can be simplified as:

$$\frac{y_{s(Pier)}}{a} = \alpha_1\left(\beta_1 \cdot Fr_{(pier)} - Fr_{c(pier)}\right)^{\chi 1} \tag{6}$$

The constants $\alpha_{\square\square\square}, \beta_{\square\square\square}$ and $\chi_{\square\square\square}$ were determined experimentally by curve fitting, and the prediction equation is:

$$\frac{y_{s(Pier)}}{a} = 2.2\left(2.6 \cdot Fr_{(pier)} - Fr_{c(pier)}\right)^{0.7} \tag{7}$$

6.3 Complex pier scour

The data for complex piers were collected from Li (2002), and re-analyzed to find the correction factors for the effects of pier shape, shallow water, the aspect ratio of rectangular pier, attack angle, and pier spacing. The equation for a complex pier is:

$$\frac{y_{s(Pier)}}{a'} = 2.2 \cdot K_w \cdot K_1 \cdot K_L \cdot K_{sp}\left(2.6 \cdot Fr_{(pier)} - Fr_{c(pier)}\right)^{0.7} \tag{8}$$

where $Fr_{(pier)}$ is Froude number based on approach velocity and *a'*, and $Fr_{c(pier)}$ is Froude number based on critical velocity and *a'*.

$$K_w = \begin{cases} 0.89\left(\dfrac{y_1}{a'}\right)^{0.33} & \text{, for } \dfrac{y_1}{a'} < 1.43 \\ 1.0 & \text{, else} \end{cases}$$

$$K_1 = \begin{cases} 1.0 & \text{, for } \theta > 30° \\ \text{Value in Table 1} & \text{, else} \end{cases}$$

$$K_L = 1.0, \quad \text{for whole range of } L/a$$

$$K_{sp} = \begin{cases} 2.9\left(\dfrac{S}{a'}\right)^{-0.91} & \text{, for } \dfrac{S}{a'} < 3.42 \\ 1.0 & \text{, else} \end{cases}$$

$$Fr_{(pier)}\left(=\frac{V_1}{\sqrt{g \cdot a'}}\right),\ Fr_{c(pier)} = \frac{V_c}{\sqrt{g \cdot a'}},\ a' = a\left(\cos\theta + \frac{L}{a} \cdot \sin\theta\right)$$

Table 1 Correction factor of pier nose shape (K_1) (Richardson et al., 2001).

Shape of pier nose	K_1	Shape of pier nose	K_1
Square nose	1.1	Circular cylinder	1.0
Round nose	1.0	Sharp nose	0.9

7. CONTRACTION SCOUR

Li (2002) conducted contraction scour experiments. He used the rectangular channel, vertical walls with different transition angel and contraction length, and Porcelain clay for experiments. He found that the maximum contraction scour depth was independent of the shape of the contraction, but dependent on the discharge and contraction ratio. He proposed two contraction scour equations in cohesive soil. One is the maximum contraction scour equation in cohesive soil (Eq. (9)), and the other is the uniform contraction scour equation (Eq. (10)).

$$\frac{y_{s(Cont)}}{y_1} = 1.9\left(1.38\frac{L_1}{L_2}Fr_1 - Fr_c\right) \tag{9}$$

$$\frac{y_{s(uni\_Cont)}}{y_1} = 1.41\left(1.31\frac{L_1}{L_2}Fr_1 - Fr_c\right) \tag{10}$$

where $y_{s(Cont)}$ is the maximum contraction scour depth, y_1 is the approach water depth, L_1 is the channel width in the approach section, L_2 is the channel width in the bridge section, $Fr_1\left(=\frac{V_1}{\sqrt{gy_1}}\right)$ is Froude number in the contracted section, and $Fr_c\left(=\frac{V_c}{\sqrt{gy_1}}\right)$ is the critical Froude number

A very simple geometry (a rectangular channel and vertical walls) was used in Li's research. Another study was conducted by Oh (2009) who included compound channels, rectangular channels, a Wing-wall abutment, and two types of Spill-through abutment. An analysis using databases in Li (2002) and Oh (2009) was conducted.

7.1 Dimensional analysis

The variables affecting contraction scour can be listed as:

$$y_{s(Cont)} = f(y_{m1}, g, V_1, C_R, sh, W_a) \tag{11}$$

Dimensional analysis yields the following dimensionless parameters:

$$\frac{y_{s(Cont)}}{y_{m1}} = f\left(Fr_{m1}, Fr_{mc}, C_R, K_{sh}, K_{CL}\right) \tag{12}$$

where y_{m1} is the main channel depth in the approach section, $C_R\left(=(Q - Q_{block})/Q\right)$ is contraction ratio, $Fr_{m2}\left(=\frac{V_1/C_R}{\sqrt{gy_{m1}}}\right)$ is Froude number in the main channel at bridge section, $Fr_{mc}\left(=\frac{V_{mc}}{\sqrt{gy_{m1}}} = \frac{\sqrt{\tau_c/\rho}}{gny_{m1}^{1/3}}\right)$ is the critical Froude number in the main channel of the bridge section, Q is the total discharge, Q_{block} is the discharge blocked by the approach embankment, W_a is the contraction length, K_{sh} is the correction factor of contraction shape, K_{CL} is the correction factor of contraction length

Since the contraction scour happens only when the velocity is larger than the critical velocity, the maximum contraction scour equation is:

$$\frac{y_{s(Cont)}}{y_{m1}} = K_{sh} \cdot K_{CL} \cdot \alpha_2 \left(\beta_2 Fr_{m2} - Fr_{mc}\right)^{\gamma 2} \quad (13)$$

where α_2, β_2 and χ_2 are constant. Note that the amplification factor β_2 is necessary to consider the influence of turbulence and should be always bigger than 1.0

7.2 Prediction equation

It was found that the contraction scour depth normalized by the water depth was linearly dependent on the difference in the Froude numbers, and was independent of the contraction length and shape after data regression. The prediction equation for the maximum contraction scour depth and the uniform contraction scour depth for both rectangular channel and compound channel can be expressed as Eq. (13) and Eq. (14), respectively.

$$\frac{y_{s(Cont)}}{y_{m1}} = 1.27\left(1.83 Fr_{m2} - Fr_{mc}\right) \quad (14)$$

$$\frac{y_{s(uni\_Cont)}}{y_{m1}} = 0.94\left(1.83 Fr_{m2} - Fr_{mc}\right) \quad (15)$$

7.3 Prediction equation for HEC-RAS users

Engineers often use numerical analyses to calculate the velocity needed in bridge design. HEC-RAS is one popular software package. A new method using the velocity calculated by HEC-RAS at the contracted section is suggested for the HEC-RAS users.

The contraction scour equation using HEC-RAS results can be expressed as

$$\frac{y_{s(Cont)}}{y_{m1}} = \alpha_2 \left(\beta_2 Fr_{m2\_HEC} - Fr_{mc}\right) \quad (16)$$

where $Fr_{m2\_HEC}\left(=\frac{V_{2\_HEC}}{\sqrt{g y_{m1}}}\right)$, V_{2_HEC} is the velocity in the main channel at the bridge section by HEC-RAS calculation.

Another data regression using flume test results and HEC-RAS results yielded Eq. (17) for the maximum contraction scour, and Eq. (18) for the uniform contraction scour.

$$\frac{y_{s(Cont)}}{y_{m1}} = 2.21\left(1.31 Fr_{m2\_HEC} - Fr_{mc}\right) \quad (17)$$

$$\frac{y_{s(uni\_Cont)}}{y_{m1}} = 1.66\left(1.31 Fr_{m2\_HEC} - Fr_{mc}\right) \quad (18)$$

Note that the amplification factor β_2 in Eq. (17) and Eq. (18) is smaller than that in Eq. (14) and Eq. (15) because the calculated velocity V_{2_HEC} is always larger than $V_{m2}\left(=V_1 / C_R\right)$ because the water depth decrease at the bridge section is taken into consideration in one method and not the other.

8. ABUTMENT SCOUR

Briaud et al. (2009) conducted 18 large scale flume tests using Porcelain clay for channel material. The flume used for the tests is 45.7 m (150 ft) long, 3.05 m (10 ft) deep, and 3.66 m (12ft) wide. In the research, the hydraulic condition, the channel geometry, the shape of abutment, the length of abutment and the abutment alignment were varied to simulate possible conditions that should be considered for bridge design. The method selected for converting the hydraulic data to the local velocity around the abutment was the approach used in Maryland SHA Bridge Scour Program (ABSCOUR, 2006).

$$V_{f2} = \begin{cases} \dfrac{Q}{A_2}, \text{for short setback } \left((L_f - L') \le 5 y_{m1}\right) \\ \dfrac{Q_{fp1}}{A_{f2}}, \text{for long setback } \left(L' \le 0.25 L_f\right) \\ \text{otherwise use a linearly interpolated velocity between} \\ \dfrac{Q}{A_2} \text{ for } (L_f - L') = 5 y_{m2} \text{ and } \dfrac{Q_{fp1}}{A_{f2}} \text{ for } L' = 0.25 L_f \end{cases} \quad (19)$$

where Q_{fp1} is the discharge on the floodplain at the approach section immediately upstream of the abutment, A_2 is total flow area at the contracted section, A_{f2} is the flow area on the floodplain at the contracted section, and L_f is the width of floodplain, L' is the length of abutment

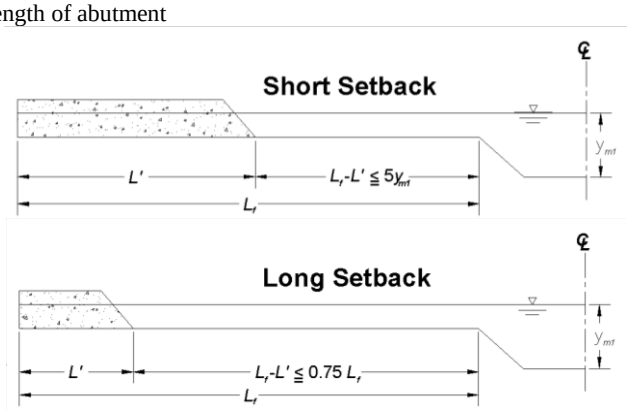

Figure 7 Definition of degree of setback.

8.1 Dimensional analysis

Variables affecting the abutment scour depth are listed in Eq. (20). These variables can be rewritten in dimensionless variables in Eq. (21).

$$y_{s(Abut)} = f(y_{m1}, y_{f1}, L_f, L', \beta_a, \theta, g, V_{f2}, \mu, V_{fc}) \quad (20)$$

$$\frac{y_{s(Abut)}}{y_{f1}} = f\left(\frac{L_f - L'}{y_{f1}}, \beta_a, \theta, Fr_{f2}, Fr_{fc}, \mathrm{Re}_{f2}\right) \quad (21)$$

where β_a is the abutment slope, θ is the alignment angle of abutment, $Fr_{f2} = \frac{V_{f2}}{\sqrt{g y_{f1}}}$, $Fr_{fc} = \frac{V_{fc}}{\sqrt{g y_{f1}}} = \frac{\sqrt{\tau_c / \rho}}{g n y_{f1}^{1/3}}$, $\mathrm{Re}_{f2} = \frac{\rho y_{f1} V_{f2}}{\mu}$, μ is the viscosity of water

The abutment scour equation also can be expressed with the form of Froude number difference like pier scour equation and contraction scour equation:

$$\frac{y_{s(Abut)}}{y_{f1}} = K_1 \cdot K_2 \cdot K_L \cdot K_G \cdot K_{\mathrm{Re}} \cdot \alpha_3 \cdot \left(\beta_3 \cdot Fr_{f2} - Fr_{fc}\right)^{\chi 3} \quad (22)$$

where K_1 is the correction factor of the abutment shape, K_2 is the correction factor of the abutment skew angle, K_L is the correction factor of the abutment location, K_G is the correction factor of channel geometry, K_{Re} is the correction factor of Reynolds number effect, and α_3, β_3 and χ_3 are constant.

8.2 Prediction equation

The three constants (α_3, β_3 and χ_3) and four correction factors (K_1, K_2, K_L K_G) were obtained after data regression using flume test results:

$$\frac{y_{s(Abut)}}{y_{f1}} = K_1 \cdot K_2 \cdot K_L \cdot K_G \cdot 7.94 \cdot \left(1.65 \cdot Fr_{f2} - Fr_{fc}\right) \qquad (23)$$

$$K_1 = \begin{cases} 1.22 & \text{for Vertical-wall abutment} \\ 1.0 & \text{for Wing-wall abutment} \\ 0.73 & \text{for Spill-through abutment with 2:1 Slope} \\ 0.59 & \text{for Spill-through abutment with 3:1 Slope} \end{cases}$$

$$K_2 = \begin{cases} 1.0 - 0.005\left|\theta - 90°\right| & for\ 60° \le \theta \le 120° \\ 0.85 & otherwise \end{cases}$$

$$K_G = \begin{cases} 1.0 & \text{for compound channel} \\ 0.42 & \text{for rectangular channel} \end{cases}$$

$$K_L = \begin{cases} -0.23\dfrac{L_f - L'}{y_{f1}} + 1.35 & \text{for } \dfrac{L_f - L'}{y_{f1}} < 1.5 \\ 1.0 & \text{otherwise} \end{cases}$$

8.3 Reynolds effect

Eq. (23) fits well to the flume test results in Briaud et al (2009). However it underestimates the scour depth for small scale laboratory tests and overestimates for large scale such as field data. The main cause for this discrepancy is the effect of local Reynolds number Re_{f2}, defined as $\mathrm{Re}_{f2} = \rho y_{f1} V_{f2} / \mu$. Indeed the Froude number was matched with the field scale in the laboratory test but not the Reynolds number as it is not possible to do both for a given fluid. Therefore there was a need to take care of the influence of the Reynolds number.

Table 2 Range of Reynolds numbers (Re_{f2}) in each study.

	Froehlich (1989)	Sturm (2004)	Briaud et al. (2009)	Benedict et al. (2006)
Min. Re_{f2}	7,425	8,433	102,511	143,500
Max. Re_{f2}	71,133	55,451	322,681	11,436,281
Avg. Re_{f2}	50,073	28,248	219,837	2,782,622

Fig. 8 shows the effect of Reynolds number in maximum abutment scour depth. In order to find the Reynolds number effect, several points from laboratory test results, such as Froehlich (1989) and Strum (2004), were selected. Note that the database from Benedict et al. (2006) was not used because the accuracy of data from field measurements is much lower than that of laboratory test results. According to the relationship in Fig. 8, the effect of Reynolds number is:

$$K_{\mathrm{Re}} = \frac{1}{0.0327 \cdot \mathrm{Re}_{f2}^{0.278}} = 30\mathrm{Re}_{f2}^{-0.28} \qquad (24)$$

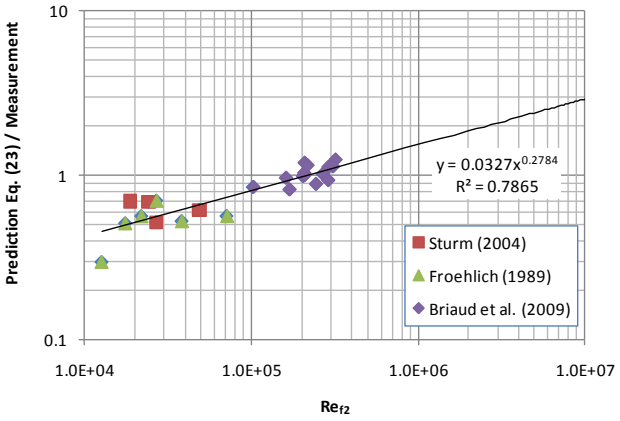

Figure 8 Effect of Reynolds number in maximum abutment scour.

The maximum abutment scour prediction equation considering the effect of Reynolds number is:

$$\frac{y_{s(Abut)}}{y_{f1}} = K_1 \cdot K_2 \cdot K_L \cdot K_G \cdot K_{\mathrm{Re}} \cdot 7.94 \cdot \left(1.65 \cdot Fr_{f2} - Fr_{fc}\right) = K_1 \cdot K_2 \cdot K_L \cdot K_G \cdot 243 \cdot \mathrm{Re}_{f2}^{-0.28} \cdot \left(1.65 \cdot Fr_{f2} - Fr_{fc}\right) \qquad (25)$$

9. TIME DEPENDENT PREDICTIONS

The scour phenomenon in cohesive soils is much slower and more dependent on soil properties than that in cohesionless soils. Applying the equations for cohesionless soils to cohesive soils without the consideration of time yields overly conservative scour depths. Therefore, a scour analysis method for cohesive materials needs to consider the effect of time and soil properties as well as hydraulic parameters. The SRICOS (Scour Rate In COhesive Soils) method was developed to predict the scour depth versus time around a cylindrical bridge pier founded in cohesive soils (Briaud et al., 1999), and has been developed to predict all possible scour types in reality.

9.1 Basic concept of SRICOS method

The SRICOS method uses tow basic parameters: the maximum scour depth (y_s) and the initial scour rate $\left(\dot{z}_i\right)$. The two are then linked by a hyperbolic model which describes the scour depth vs. time curve. The procedure for the SRICOS method consists of the following steps.

1) Obtain standard 76.2 mm diameter Shelby tube samples as close to the bridge support as possible.
2) Test the sample in the EFA to get the erodibility curve ($\dot{z}$ vs. τ). where $\dot{z}$ is the erosion rate and τ is the interface shear stress.
3) Determine the maximum shear stress τ_{max} at the beginning of the scour process.
4) Obtain the initial scour rate $\left(\dot{z}_i\right)$ corresponding to τ_{max}.
5) Develop the complete scour depth y_s vs. t curve.
6) Predict the depth of scour by reading the y_s vs. t curve at the time corresponding to the duration of the flood using

$$y_s(t) = \frac{t}{\frac{1}{\dot{z}_i} + \frac{t}{y_s}} \tag{26}$$

where t is time (hour), y_s is the maximum scour depth, $\dot{z}_i$ is the initial scour rate

9.2 Multi-flood system and multi-layer system

Kwak (2000) developed the SRICOS method for multi-flood and multi-layer systems to apply it to actual cases of scour. His concepts are:

9.2.1 Multi-flood system

The hydrograph of a river indicates how the velocity varies with time. The fundamental basis of the accumulation algorithms is that the velocity histogram is a step function with a constant velocity value for each time step. For example, a flood followed by a bigger flood in a uniform soil is first considered (Fig. 9). Flood 1 lasts a time t_1, with a velocity V_1, and Flood 2 lasts time t_2 with a velocity V_1. A scour depth $y_{s1}(t_1)$ is reached at a time t_1 (Point A on Fig. 9 (b)) after Flood 1.

$$y_{s1}(t_1) = \frac{t_1}{\frac{1}{\dot{z}_{i1}} + \frac{t_1}{y_{s1}}} \tag{27}$$

The scour depth $y_{s1}(t_1)$ could have been created by Flood 2 in a time t_e such that:

$$y_{s1}(t_1) = \frac{t_e}{\frac{1}{\dot{z}_{i2}} + \frac{t_e}{y_{s2}}} \tag{28}$$

Therefore the equivalent time te is:

$$t_e = \frac{t_1}{\frac{\dot{z}_{i2}}{\dot{z}_{i1}} + t_1 \dot{z}_{i2}\left(\frac{1}{y_{s1}} - \frac{1}{y_{s2}}\right)} \tag{29}$$

When Flood 2 starts, even though $y_{s1}(t_1)$ has occurred due to Flood 1 during t_1, $y_{s1}(t_1)$ is equal to $y_{s2}(t_e)$ due to Flood 2 during the equivalent time t_e. The y_s vs. t curve proceeds from point B on Fig. 9 (c) to point C after t_2. The y_s vs. t curve for the sequence of Flood 1 and 2 follows the path OA on the curve during Flood 1, and then switches to BC on the curve during flood 2. This is shown as the curve OAC on Fig. 9 (d).

In the opposite case where a flood is followed by a smaller flood the same approach can be used except that if $y_{s1}(t)$ is bigger than y_{s2}, a smaller flood cannot develop any additional scour.

In the general case, the complete velocity hydrograph is divided into a series of partial flood events lasting Δt. The scour depth due to floods in the hydrograph is calculated by following the procedure in Fig. 9 (d).

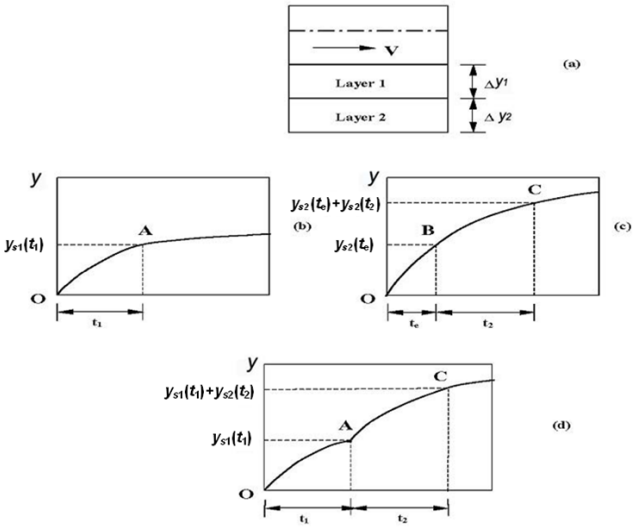

Figure 9 Scour due to a sequence of two flood events.

9.2.2 Multi-layer system

In the multi-flood system analysis, the soil is assumed to be uniform. In reality, the soil can involve different layers and the layer characteristics can vary significantly with depth. Therefore, it is necessary to have an accumulation process which can handle the case of a multi-layer system. This problem is that a flow with a constant velocity V where a channel bottom consists of a first layer with a thickness of Δy_1 and a second layer with a thickness of Δy_2 (Fig. 10 (a)). The y_s vs. t curves for layer 1 and layer 2 are given by Eq. (27) and Eq. (28) (Fig. 10 (b), Fig. 10 (c)). If y_{s1} exceeds the thicknessΔy_1, then layer 2 will also be involved in the scour process. In this case, the scour depth y_{s1} (t_1) (=Δy_1) (point A on Fig. 10 (b)) in layer 1 is reached after a time t1, and it is equivalent to scour depth on layer 2 during equivalent time te (point B on Fig. 10 (c)). Therefore, when layer 2 starts to erode, the y_s vs. t curve proceeds from point B to C on Fig. 10 (c). The combined scour process for the two-layer system corresponds to the path OAC on Fig. 10 (d).

In reality, there may be a series of soil layers with different erosion functions. The computations proceed by stepping forward in time. The time steps are Δt long, the velocity is the one for the corresponding flood event, and the erosion function ($\dot{z}$ vs τ) is the one for the soil layer corresponding to the current scour depth (bottom of the scour hole). When Δt is such that the scour depth enters a new soil layer, the computations follow the process described in Fig. 10 (d).

$$k_R = 0.62 + 0.38\left(A_1/A_2\right)^{1.75} \qquad k_\alpha = 1.0 + 0.9\left(\alpha/90\right)^{1.5}$$

$$k_{wa} = \begin{cases} 0.77 + 1.36\left(\dfrac{W_a}{L'_{left} + L'_{right}}\right) - 1.98\left(\dfrac{W_a}{L'_{left} + L'_{right}}\right)^2 & \text{, for } \dfrac{W_a}{L'_{left} + L'_{right}} \le 0.35 \\ 1.0 & \text{, otherwise} \end{cases}$$

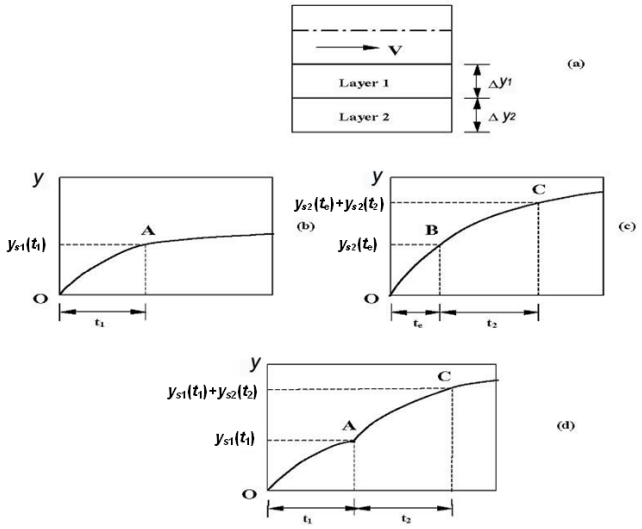

Figure 10 Scour on multi-layers.

9.3 Maximum shear stress around pier

Wei et al. (1997) performed a series of 3D numerical simulation for a constant velocity flow in a deep water condition, and then developed Eq. (30) for the maximum shear stress occurring around a cylindrical pier. The equation is:

$$\tau_{\max(Pier)} = 0.094\rho V_1^2\left[\frac{1}{\log \mathrm{Re}} - \frac{1}{10}\right] \tag{30}$$

Nurtjahyo (2003) conducted a series of 3D numerical simulation by varying water depth, pier spacing, pier shape, and attack angle, and found several correction factors, which are applicable to Eq. (30), for shallow water depth effect, pier spacing effect, pier shape effect and attack angle effect. Eq. (31) was proposed for the maximum shear stress occurring around a complex pier.

$$\tau_{\max(pier)} = k_w k_{sh} k_{sp} k_\theta \cdot 0.094\rho V_1^2\left[\frac{1}{\log \mathrm{Re}} - \frac{1}{10}\right] \tag{31}$$

$$k_w = 1 + 16\exp\left(-4y/a\right) \qquad k_{sh} = 1.15 + 7\exp\left(-4L/a\right)$$

$$k_\theta = 1 + 1.5\left(\theta/90\right)^{0.57} \qquad k_{sp} = 1 + 5\exp\left(-1.1S/a\right)$$

where k_w, is the correction factor of water depth, k_{sp}, is the correction factor of pier spacing, k_{sh}, is the correction factor of pier shape, k_θ, is the correction factor of attack angle

9.4 Maximum shear stress in a contraction zone

Nurtjahyo (2003) studied the maximum shear stress in a contraction zone by conducting another series of 3D numerical simulation in a contracted rectangular channel, and developed Eq. (32). Eq. (32) was developed by correcting the maximum shear stress equation at the bottom of an open channel without contraction (Munson et al., 1990).

$$\tau_{\max(Cont)} = k_R k_{Wa} k_\alpha k_w \rho g n^2 V_1^2 R_h^{-\frac{1}{3}} \tag{32}$$

where R_h is the hydraulic radius, α is the contraction transition angle (in degree), W_a is the top width of the abutment, A_1 is the channel area at approach section, A_2 is the channel area at bridge section, L'_{left} is the length of left bridge embankment, L'_{right} is the length of right bridge embankment, k_R is the correction factor of the contraction ratio, k_α is the correction factor of the transition angle, k_{wa} is the correction factor of the contraction length, and k_w is the correction factor of the water depth and it is 1.0 for all conditions

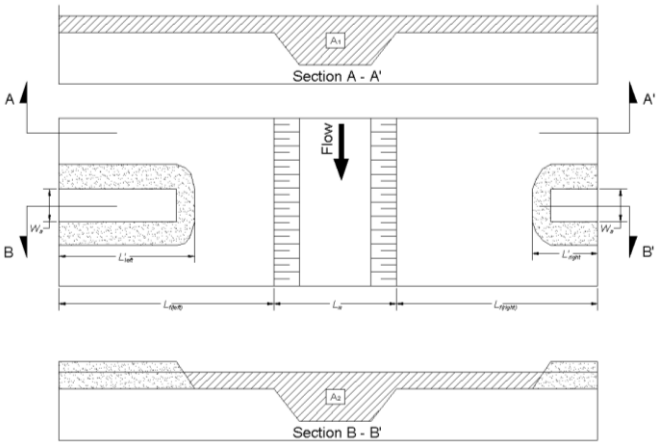

Figure 11 Definition of parameters in the contraction scour.

9.5 Maximum shear stress around the toe of an abutment

Chen (2008) conducted a series of 3D numerical simulation to study the maximum shear stress around the toe of an abutment, and developed Eq. (33).

$$\tau_{\max(Abut)} = 12.45 k_{Cr} k_{sh} k_{Fr} k_s k_{sk} k_L k_o \rho V_1^2 \mathrm{Re}^{-0.45} \tag{33}$$

$$k_{Cr} = 3.65\frac{q_2}{q_1} - 2.91 \quad , \qquad k_{sh} = 0.85 \times \left(\frac{L'}{W_a}\right)^{-0.24} ,$$

$$k_{Fr} = \begin{cases} 2.07Fr + 0.8 & \text{for } Fr > 0.1 \\ 1.0 & \text{for } Fr \le 0.1 \end{cases} ,$$

$$k_s = \begin{cases} 1.0 & \text{vertical-wall abutment} \\ 0.65 & \text{wing-wall abutment} \\ 0.58 & \text{spill-through abutment} \end{cases} ,$$

$$k_L = \begin{cases} 1.0 & \text{for} \left(L_f - L^{'}\right) / y_f \le -2 \\ 0.6(L_f - L^{'}) / y_f + 1.2 & \text{for} -2 < (L_f - L^{'}) / y_f \le 0 \\ -1.2(L_f - L^{'}) / y_f + 1.2 & \text{for} 0 < (L_f - L^{'}) / y_f \le 1 \\ 1.0 & \text{for} 1 \le (L_f - L^{'}) / y_f \end{cases},$$

$$k_o = \begin{cases} 0.92 \cdot \left(d_1 / d_{deck}\right) + 1.0 & \text{for } d_1 / d_{deck} < 1.0 \\ 0.21\left(d_1 / d_{deck}\right)^2 - 1.27\left(d_1 / d_{deck}\right) + 2.97 & \text{for } 1.0 \le d_1 / d_{deck} \le 3.0 \\ 1.0 & \text{for } 3.0 < d_1 / d_{deck} \end{cases}$$

where $\mathrm{Re}\left(= V_1 W_a / \nu\right)$ is the Reynolds number defined with respect to the top width of the abutment, $q_1\left(= V_1 \cdot y_1\right)$ is the unit discharge at the approach section, $q_2\left(= V_1 \cdot y_1 \cdot A_1 / A_2\right)$ is the unit discharge at the bridge section, d_1 is the distance from the water surface to the low chord of the bridge at the upstream face of the bridge, d_{deck} is the thickness of the bridge deck, k_{sh} is the correction factor of the aspect ratio of the approach embankment, k_{Fr} is the correction factor of Froude number, k_s is the correction factor of the abutment shape, $k_{sk}\left(=1.0\right)$ is the correction factor of abutment alignment, k_o is the correction factor of overtopping

10. PROBABILITY APPROACH

All methods mentioned above determine the scour depth at the end of a given sequence of daily discharge values. Wang (2004) suggested a methodology to predict the scour depth at the end of a future hydrograph on a probabilistic basis. In his research, he set up a Monte Carlo simulation procedure by assuming that the hydrograph can be modeled as a stochastic process. His methodology to prepare future hydrographs depended on whether a hydrograph existed or only Q_{100} and Q_{500} existed.

10.1 Existing hydrograph method

The daily discharge, Q in the hydrograph, is considered as a random, uncorrelated variable. A suitable distribution (Log normal) is fitted to the discharge data from the hydrographs. The mean and standard deviation of the Lognormal distribution μ_y and σ_y are determined from the mean and the standard deviation of the flow values, μ_Q and σ_Q by:

$$\mu_y = \frac{1}{2} Log\left[\frac{\mu_Q^{\,2}}{1 + \left(\frac{\sigma_Q}{\mu_Q}\right)^2}\right] \tag{34}$$

$$\sigma_y = \sqrt{Log\left[1 + \left(\frac{\sigma_Q}{\mu_Q}\right)^2\right]} \tag{35}$$

The basic procedures of existing hydrograph approach are:

1) Calculate the mean μ_Q and standard deviation σ_Q of the daily stream flow values in existing hydrograph.
2) Calculate the log-normal mean μ_y and standard deviation σ_y of the daily stream flow values by using Eq. (34) and Eq. (35).
3) Using the cumulative distribution function and a random number generator, a large number of equally likely future hydrograph are generated.

10.2 Q_{100} and Q_{500} method

If a hydrograph does not exist at the bridge, but the Q_{100} and Q_{500} are known values, the parameters of the Lognormal Distribution (mean value and standard deviation) can be calculated using the conditions:

$$\mathrm{Prob}\left[Q > Q_{100}\right] = 0.01\left(\text{per year}\right) = 1/36500 \ \left(\text{per day}\right) \tag{36}$$

$$\mathrm{Prob}\left[Q > Q_{500}\right] = 0.002\left(\text{per year}\right) = 1/182500 \ \left(\text{per day}\right) \tag{37}$$

The function Prob[$Q < Q_x$] has tow constants: μ_y and σ_y. Therefore the tow conditions [Eq. (36) and Eq. (37)] give the values of μ_y and σ_y. and the Lognormal distribution is completely defined. Hence, the basic procedures of Q_{100} and Q_{500} approach will be:

1) Calculate the Lognormal mean μ_y and standard deviation σ_y of the daily discharge by using Eq. (36) and Eq.(37).
2) Using the cumulative distribution function and a random number generator, a large number of equally likely future hydrograph are generated.

10.3 Probability of exceedance

The probability of exceedance, $\underline{P}$, of the design flood with a given return period T_r depends on the design life L_t of a structure.

$$\underline{P} = 1 - \left(1 - 1/T_r\right)^{L_t} \tag{38}$$

If the design life of the bridge is 75 years, the probability that the flood with a return period of 100 year will be exceeded during the 75 year design life is 53% according to Eq. (38) and that probability is 14% for the 500 year flood. Only when one gets to the 10,000 year flood does the probability get to be lower than 1% (0.75%). Therefore looking at those numbers alone, it seems desirable to use the 10,000 year flood for design purposes. This flood is used in design in the Netherlands for regions of the country deemed critical. The USA uses the 100 and 500 year flood for design purposes in hydraulic engineering; this leads to probabilities of exceedance which are in the tens of percent. By comparison, the structural engineers use a probability of exceedance of about 0.1% for the design of bridge beams (LRFD target), and judging from measured vs. predicted pile capacity data bases (Briaud, Tucker, 1988) the geotechnical engineer uses a probability of exceedance of the order of a few percent. While these numbers can be debated, it is relatively clear that these different fields of civil engineering operate at vastly different probability of exceedance levels. There is a need to document these different levels, agree on a target level, and then operate at that common level. Note that risk is associated with the product of the probability of occurrence and the value of the consequence. As such, the probability of exceedance target should vary with the consequence of the failure.

11. SRICOS-EFA METHOD

Since cohesive soils may be scoured so much more slowly than cohesionless soils, the scour rate should be included for scour prediction. The SRICOS-EFA method has been developed for this reason with consideration of the time effect, the soil properties and the hydraulic parameters. The SRICOS-EFA computer program is programmed to calculate three types of scour depth: pier, contraction, and abutment. It can be downloaded for free at https://ceprofs.civil.tamu.edu/briaud/. The procedure of the

SRICOS-EFA method is outlined in Fig. 12, and it is simply summarized as:

1) Collect samples at the site.
2) Test the samples in the EFA to get the erodibility curves or use the proposed soil erosion charts.
3) Describe the geometry of the abutment (length, width, shape and alignment angle), and pier (nose shape, width, length, skew angle).
4) Describe the geometry of the river (main channel width, flood plain width left, flood plain width right, main channel to flood plain transition slope, flood plain bank slope, Manning coefficient and longitudinal slope of the river).
5) Input the flow hydrograph.
6) Run HEC-RAS to obtain the relationship between the flow and velocity at the bridge section, and the flow and water depth.
7) Transform the flow hydrograph into a bridge section velocity hydrograph and a water depth hydrograph.
8) Calculate the maximum scour depth for the i^{th} velocity on the hydrograph (equation (8) for pier scour, equation (13) for contraction scour, equation (24) for abutment scour).
9) Calculate the initial maximum shear stress around the abutment for the i^{th} velocity (before the scour hole development) (equation (30) for pier scour, equation (31) for contraction scour, equation (32) for abutment scour).
10) Read the initial scour rate corresponding to the initial maximum shear stress on the appropriate EFA curve.
11) Use the results of steps 8 and 10 to construct the scour depth versus time curve for the i^{th} velocity.
12) Calculate the equivalent time for the i^{th} velocity and the curve of step 11). The equivalent time for the i^{th} velocity is the time necessary for i^{th} velocity in the hydrograph to create the same scour depth as the hydrograph from the start up to the time step.
13) Read the additional scour depth contributed by the i^{th} velocity during the i^{th} time step.
14) Repeat steps 8 to 13 for the entire hydrograph.
15) Output the scour depth versus time and read the final scour depth y_{s_final} at the end of the hydrograph period.

11.1 Example

The SRICOS-EFA method is applied to predict the pier scour depth at Woodrow Wilson bridge. The soil samples taken around pier 1W at depth of 4 – 4.6 m and 10 – 10.6 m are clay with 41 % and 33 % of PI, respectively. The pier nose shape is square, and the width is 9.75 m. The erosion functions of soil samples around bridge pier are shown in Fig. 13. Fig. 14 (a) shows the measured original hydrograph, and Fig. 14 (b) is the corresponding prediction of scour depth history using the SRICOS-EFA method. The mean and standard deviation of Q of the period from 1961 to 2000 are μ_Q=354 m^3/s, and σ_Q=502 m^3/s, respectively, and the maximum discharge in the 40-year-long record was 9,702 m^3/s. In addition, at this bridge site, the Q_{100} is 12,629 m^3/s and the Q_{500} is 16,639 m^3/s.

Fig. 15 (a) shows the frequency of occurrence, and Fig. 15 (b) shows the probability of exceedance using the existing hydrograph method of probability approach. The period of synthetic hydrographs is 75 years and the iteration number is 1000.

Fig. 16 (a) shows the frequency of occurrence, and Fig. 16 (b) shows the probability of exceedance using the Q_{100} and Q_{500} method of probability approach. The period of synthetic hydrographs is 75 years and the iteration number is 1000.

12. VERIFICATION

The SRICOS-EFA method was developed to predict bridge scour depths, such as pier scour, contraction scour and abutment scour, in cohesive soils on the basis of flume tests. As with any new method, it is important to verify the method against other measurements. The databases which were used for the verification of the SRICOS-EFA method are listed in Table 3.

In order to apply these three equations to databases, and because there were no EFA test results in those databases, cohesionless soils databases were used, and the relationship between the critical shear stress of the soil and the D_{50} particle size was used to calculate the critical shear stresses of each soil. Moreover, Manning's coefficient n was calculated using Strikler's relation (n=0.013$D_{50}^{1/6}$ ≥ 0.011) for D_{50} in unit of mm.

Fig.17 and Fig. 18 show the comparison of the predicted maximum pier scour depth to the field measurements for the Froehlich database (1988), and the Muller and Lander databases (1996), respectively. Eq. (8) yields conservative scour depths compared to the field measurements. These conservative predictions may result from the fact that the erosion rate may have been slow enough that the maximum scour depth was not reached.

Fig. 19 and Fig. 20 shows the comparison between the SRICOS-EFA predictions and Gill's flume test results (1981), as well as the comparison between HEC-18 method to those same measurements. Eq. (15) is in good agreement (Fig. 19) while HEC-18 method severely under predicts the measurements (Fig. 20). Four series of abutment scour data bases are used for the verification of Eq. (25), and those are from Froehlich's (1989), Sturm (2004), Ettema et al. (2008) and Benedict et al. (2006). The comparisons of the predicted abutment scour depths with the data from these databases are shown in Fig. 21 to Fig.24. They indicate that with a factor of safety of 2, extremely few cases are under predicted. Because several of these databases are populated with coarse grained soils, it is concluded that the SRICOS-EFA method is equally applicable to fine grained soils and to coarse grained soils.

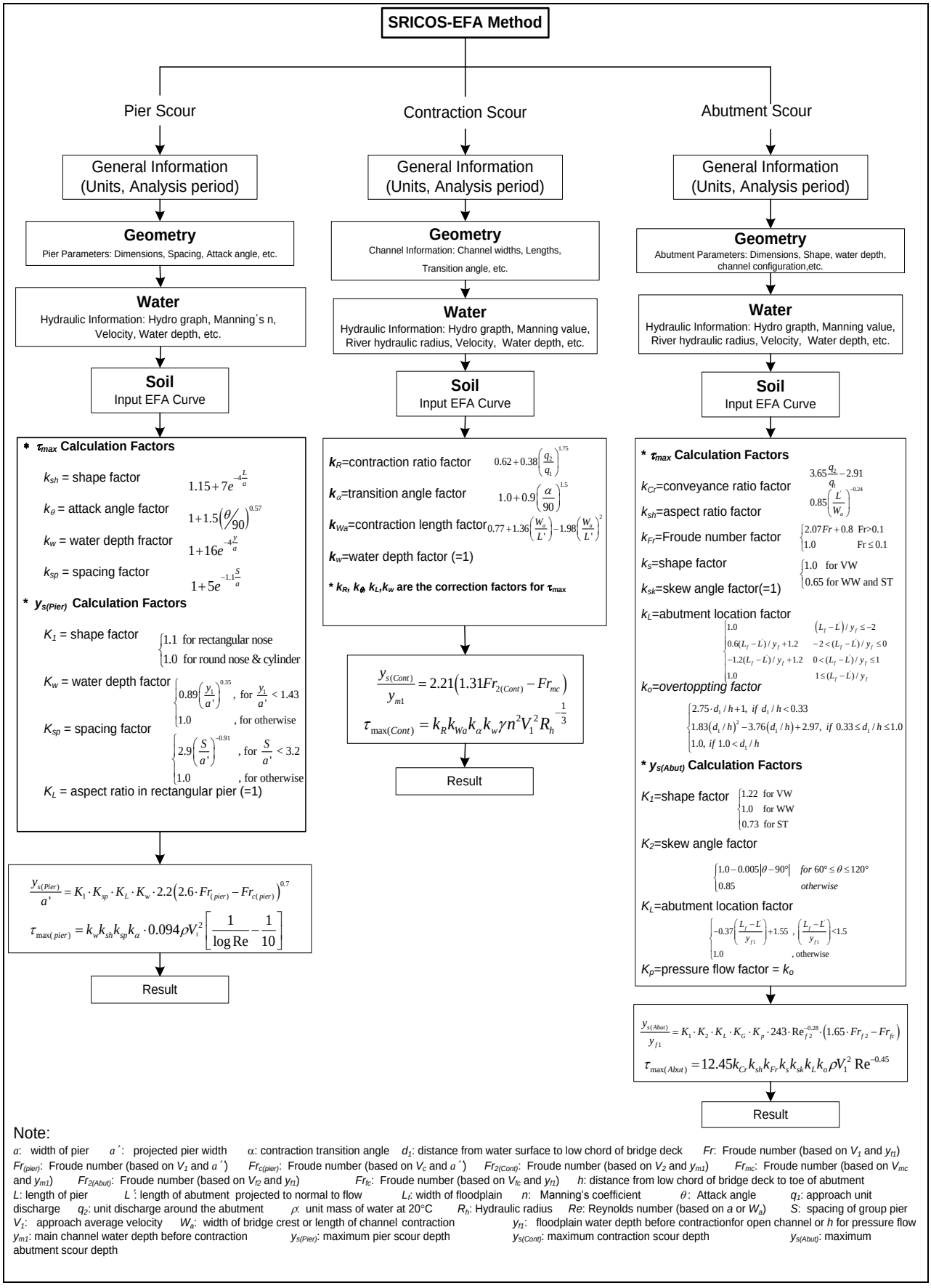

Note:

a: width of pier *a'*: projected pier width α: contraction transition angle d_1: distance from water surface to low chord of bridge deck *Fr*: Froude number (based on V_1 and y_{f1}) $Fr_{(pier)}$: Froude number (based on V_1 and *a'*) $Fr_{c(pier)}$: Froude number (based on V_c and *a'*) $Fr_{2(Cont)}$: Froude number (based on V_2 and y_{m1}) Fr_{mc}: Froude number (based on V_{mc} and y_{m1}) $Fr_{2(Abut)}$: Froude number (based on V_{f2} and y_{f1}) Fr_{fc}: Froude number (based on V_{fc} and y_{f1}) *h*: distance from low chord of bridge deck to toe of abutment *L*: length of pier *L'*: length of abutment projected to normal to flow L_f: width of floodplain *n*: Manning's coefficient θ: Attack angle q_1: approach unit discharge q_2: unit discharge around the abutment ρ: unit mass of water at 20°C R_h: Hydraulic radius *Re*: Reynolds number (based on *a* or W_a) *S*: spacing of group pier V_1: approach average velocity W_a: width of bridge crest or length of channel contraction y_{f1}: floodplain water depth before contractionfor open channel or *h* for pressure flow y_{m1}: main channel water depth before contraction $y_{s(Pier)}$: maximum pier scour depth $y_{s(Cont)}$: maximum contraction scour depth $y_{s(Abut)}$: maximum abutment scour depth

Figure 12 Procedure of SRICOS-EFA method.

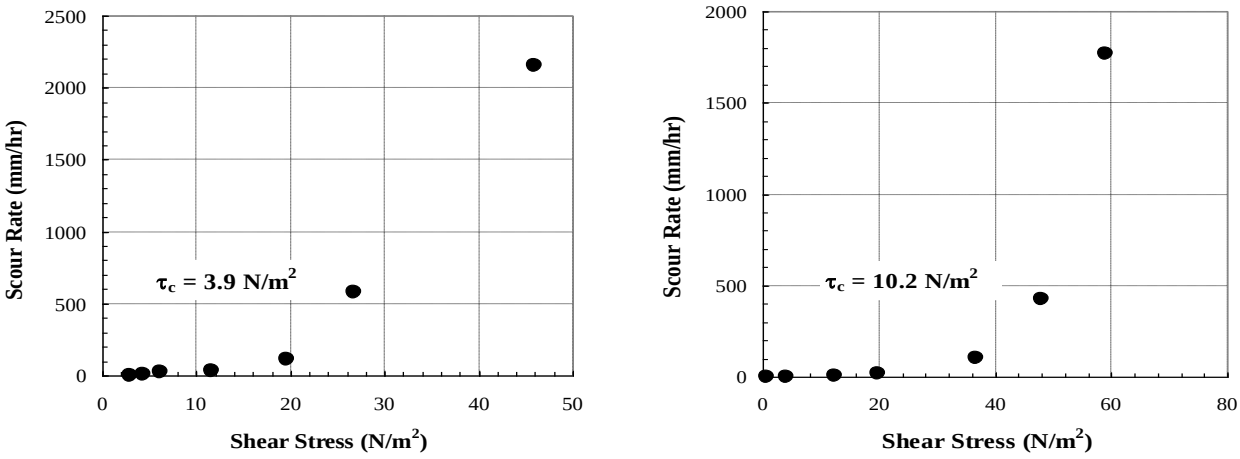

(a) at depth of 4 – 4.6 m (b) at depth of 10 – 10.6 m

Figure 13 Erosion function for a soil sample near pier 1E of the existing Woodrow Wilson bridge.

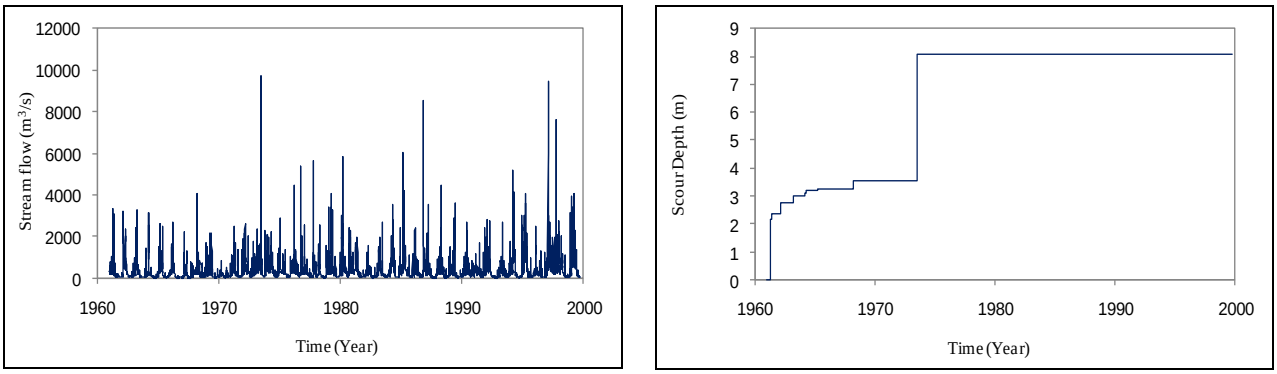

(a) Original hydrograph (b) Scour depth vs. time

Figure 14 Original hydrograph & Scour depth vs. time near Woodrow Wilson Bridge site.

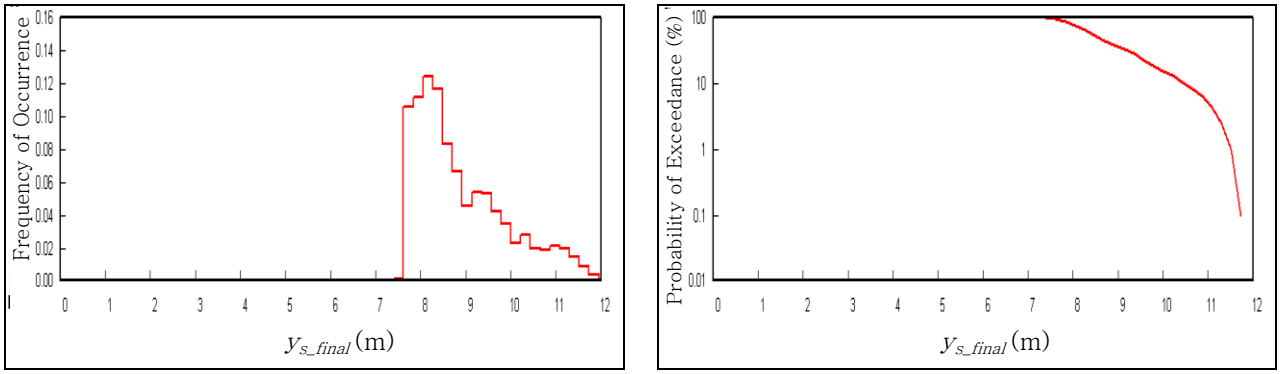

(a) Frequency of occurrence (b) Probability of exceedance

Figure 15 Scour depth prediction using existing hydrograph method of probability approach (project time = 75yrs, number of iteration = 1,000).

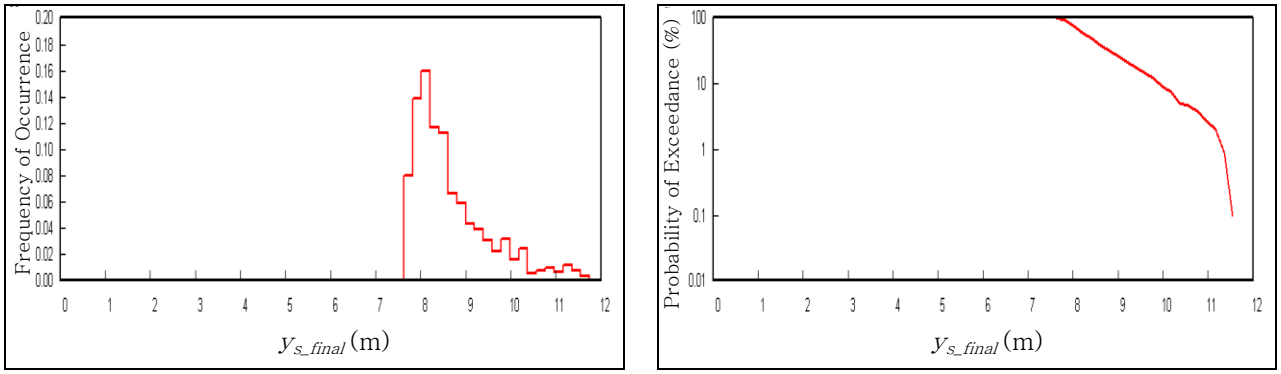

(a) Frequency of occurrence (b) Probability of exceedance

Figure 16 Scour depth prediction using Q100 and Q500 method of probability approach (project time = 75yrs, number of iteration = 1,000

Table 3 Databases for SRICOS-EFA verification.

Scour type	Database	Data type	Equation for comparison
Pier scour	Froehlich (1988) Muller and Landers (1996)	Field measurements Field measurements	Equation (8)
Contraction scour	Gill (1981)	Flume tests	Equation (15)
Abutment scour	Froehlich (1989) Strum (2004) Ettema et al. (2008) Benedict et al. (2006)	Flume tests Flume tests Flume tests Field measurements	Equation (25)

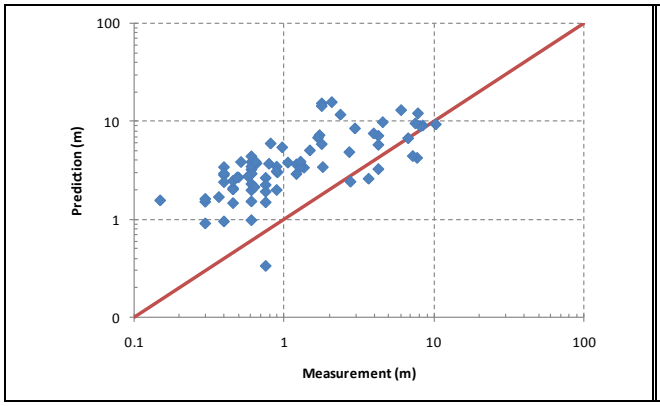

Figure 17 Prediction by Eq. (8) versus Froehlich's pier scour data base (1988).

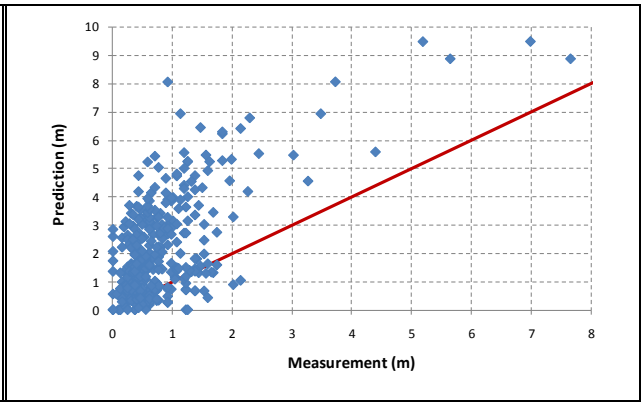

Figure 18 Prediction by Eq. (8) versus Muller and Landers' pier scour database (1996).

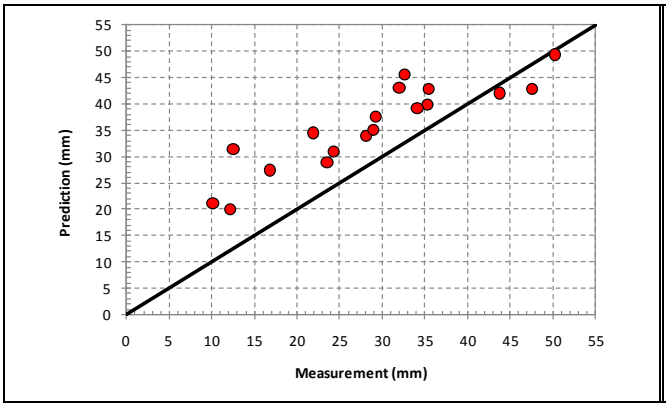

Figure 19 Prediction by Eq. (15) vs. Gill's contraction scour database (1981).

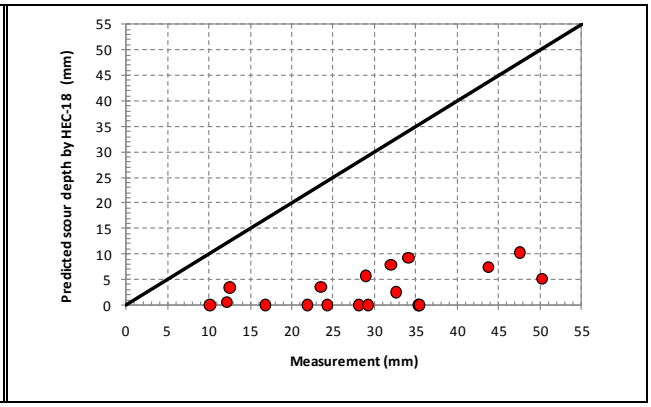

Figure 20 HEC-18 method vs. Gill's contraction scour database (1981).

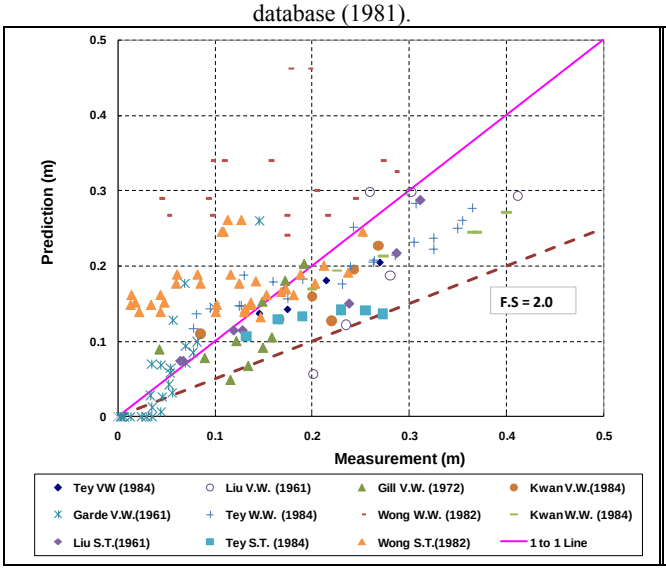

Figure 21 Prediction by Eq. (24) vs. Froehlich's abutment scour database (1989).

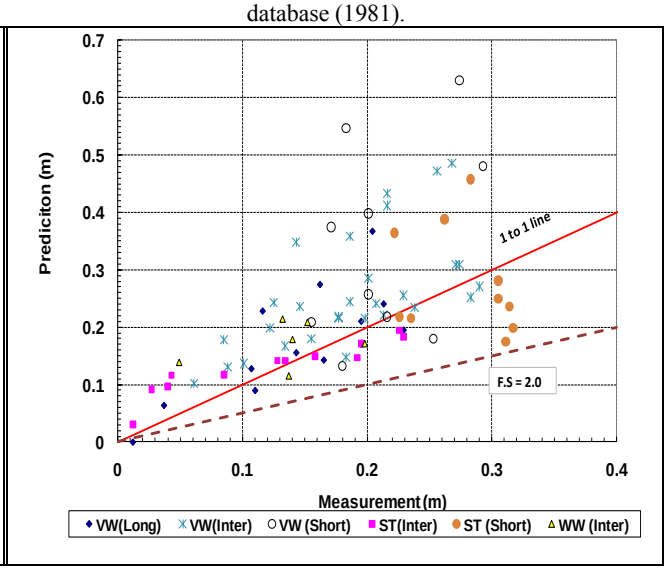

Figure 22 Prediction by Eq. (24) vs. Sturm's abutment scour database (2004).

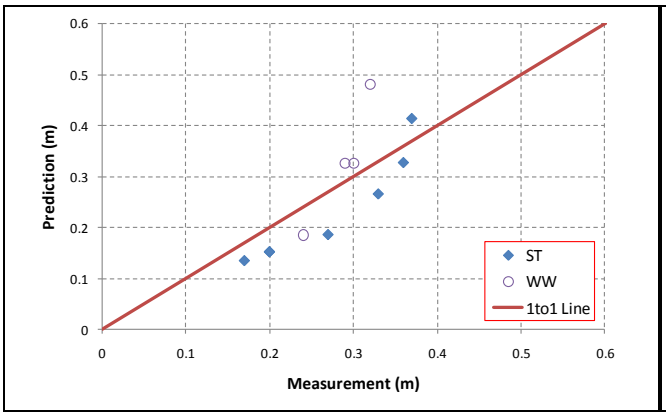

Figure 23 Prediction by Eq. (24) vs. Ettema et al.'s abutment scour database (2008).

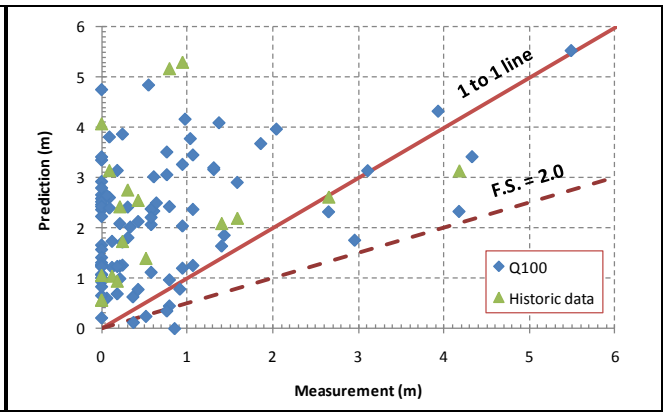

Figure 24 Prediction by Eq. (24) vs. Benedict et al.'s abutment scour database (2006).

13. REFERENCES

[1] ABSCOUR. (*Maryland SHA Bridge Scour Computer Program*), Maryland State Highway Administration, Version 8, build 1.02, compiled August 14, 2006.

[2] Benedict, S. T., and Caldwell, A. W. (2006). "Development and Evaluation of Clear-Water Pier and Contraction Scour Envelope Curves in the Coastal Plain and Piedmont Provinces of South Carolina." *U.S. Geological Survey Scientific Investigations Report 2005 - 5289*, U.S.G.S., Reston, VA, USA.

[3] Briaud, J.-L. (2008). "Case Histories in Soil and Rock Erosion: Woodrow Wilson Bridge, Brazos River Meander, Normandy Cliffs, and New Orleans Levees." *The 9th Ralph B. Peck Lecture, J. Geotech. Geoenviron. Eng.*, 134(10).

[4] Briaud, J.-L., Chen, H.-C., Chang, K.-A., Oh, S. J., and Chen, X. (2009). "Abutment Scour in Cohesive Material." *NCHRP Report 24-15 (2)*, Transportation Research Board National Research Council, Washington, DC, USA.

[5] Briaud, J.-L., Ting, F., Chen, H. C., Cao, Y., Han, S.-W., and Kwak, K. (2001). "Erosion Function Apparatus for Scour Rate Predictions." *J. Geotech. Geoenviron. Eng.*, 127(2), 105-113.

[6] Briaud, J.-L., Ting, F., Chen, H. C., Gudavalli, S. R., Kwak, K., Philogene, B., and Han, S.-W. (1999). "SRICOS: Prediction of scour rate at bridge piers." *TTI Report No. 2937-1 to the Texas DOT*, Texas A&M University, College Station, TX, USA.

[7] Briaud, J.-L., Ting, F., Chen, H. C., Gudavalli, S. R., Perugu, S., and Wei, G. (1999). "SRICOS: Prediction of scour rate in cohesive soils at bridge piers." *J. Geotech. Geoenviron. Eng.*, 125(4), 237-246.

[8] Briaud, J.-L., and Tucker, L. M. (1988). "Measured and Predicted Axial Response of 98 Piles." *J. Geotech. Eng.*, 114(9).

[9] Chen, X. (2008). "Numerical study of abutment scour in cohesive soils," Ph. D. dissertation. Texas A&M University, College Station, TX, USA.

[10] Chow, V. T., Maidment, D. R., and Mays, L. W. (1988). *Applied Hydrology*, McGraw-Hill.

[11] Ettema, R., Nakato, T., and Muste, M. (2008). "Estimation of Scour Depth at Bridge Abutment.", *NCHRP 24-20*, Transportation Research Board National Research Council, Washington, DC, USA.

[12] Froechlich, D. C. "Analysis of Onsite Measurement of Scour at Piers." *ASCE National Hydraulic Engineering Conference*, 1988, Colorado Springs, CO, USA.

[13] Froechlich, D. C. "Local Scour at Bridge Abutment." *Proceedings of National Conference on Hydraulic Engineering*, 1989, New York, NJ, USA, 13-18.

[14] Gudavalli, S. R. (1997). "Prediction model for scour rate around bridge piers in cohesive soils on the basis of flume

tests," Ph. D. dissertation. Texas A&M University, College Station, TX, USA.

[15] Kwak, K. (2000). "Prediction of scour depth versus time for bridge piers in cohesive soils in the case of multi-flood and multi-layer soil system," Ph. D. dissertation. Texas A&M University, College Station, TX, USA.

[16] Li, Y. (2002). "Bridge pier scour and contraction scour in cohesive soils on the basis of flume tests," Ph. D. dissertation. Texas A&M University, College Station, TX, USA.

[17] Moody, L. F. (1944). "Friction Factors for Pipe Flow." Transaction of the American Society of Civil Engineers, 66, Reston, Virginia, USA.

[18] Nurtjahyo, P. Y. (2003). "Chimera RANS simulations of pier scour and contraction scour in cohesive soils," Ph. D. dissertation. Texas A&M University, College Station, TX.

[19] Oh, S. J. (2009). "Experimental Study of Bridge Scour in Cohesive Soil," Ph. D. dissertation. Texas A&M University, College Station, TX, USA.

[20] Sturm, T. W. (2004). "Enhanced Abutment Scour Studies for Compound Channels.", *FHWA-RD-99-156*, Georgia Institute of Technology, School of Civil and Environmental Engineering, Atlanta, GA, USA.

[21] Wang, J. (2004). "The SRICOS-EFA method for complex pier and contraction scour," Ph. D. dissertation. Texas A&M University, College Station, TX.

[22] Wei, G., Chen, H.-C., Ting, F., Briaud, J.-L., Gudavalli, S. R., and Perugu, S. (1997). "Numerical Simulation to Study Scour Rate in Cohesive Soils." *Research Report Prepared for the Texas Department of Transportation*, Department of Civil Engineering, Texas A&M University, College Station, TX, USA

NOMENCLATURE

a	Width or diameter of pier
a'	Projected pier width perpendicular to the flow for rectangular pier
α	Contraction transition angle
A_1	Total flow area in the approach section immediately upstream of the abutment
A_2	Total flow area in the contracted section
A_{f1}	Flow area on the floodplain in the approach section immediately upstream of the abutment
A_{f2}	Flow area on the floodplain at the contracted section
C_r	Contraction ratio $C_r = (Q - Q_{blocked}) / Q$
d_1	Distance from water surface to the low chord of the bridge at upstream face of the bridge
d_{deck}	Thickness of bridge deck
D_{50}	Median diameter of sediment
Fr_1	Froude number based on V_1 and y_1
$Fr_{(Pier)}$	Froude number based on V_1 and a'
Fr_c	Critical Froude number based on V_c and y_1
$Fr_{c(Pier)}$	Critical Froude number based on V_c and a'
Fr_{f2}	Froude number based on V_{f2} and y_{f1}
Fr_{m2}	Froude number in the main channel at the bridge section
Fr_{fc}	Froude number based on V_c and y_{f1}
Fr_{mc}	Critical Froude number in the main channel at the bridge section
Fr_{m2_HEC}	Froude number based on V_{2_HEC}
g	Gravitational acceleration
k_α	Correction factor of the contraction transition angle for $\tau_{max(Cont)}$
k_{Cr}	Correction factor of discharge ratio for $\tau_{max(Abut)}$
k_{Fr}	Correction factor of Froude number for $\tau_{max(Abut)}$
k_L	Correction factor of the abutment location for $\tau_{max(Abut)}$
k_o	Correction factor of overtopping for $\tau_{max(Abut)}$
k_θ	Correction factor of attack angle for $\tau_{max(Pier)}$
k_R	Correction factor of contraction ratio for $\tau_{max(Cont)}$
k_s	Correction factor of abutment shape for $\tau_{max(Abut)}$
k_{sh}	Correction factor of aspect ratio for $\tau_{max(Abut)}$ or Correction factor of pier shape for $\tau_{max(Pier)}$
k_{sh}	Correction factor of the abutment alignment for $\tau_{max(Abut)}$
k_w	Correction factor of water depth
k_{Wa}	Correction factor of the contraction length for $\tau_{max(Cont)}$
K_1	Correction factor of pier or abutment shape for maximum abutment or pier scour depth
K_2	Correction factor of attack angle for maximum abutment or pier scour depth
K_{CL}	Correction factor of contraction length for maximum contraction scour depth
K_G	Correction factor of channel geometry for maximum abutment scour depth
K_{Re}	Correction factor of Reynolds number effect for maximum abutment scour depth

K_L	Correction factor of the abutment location for maximum abutment scour depth or correction factor of the aspect ratio of rectangular pier
K_{sh}	Correction factor of contraction shape
K_{sp}	Correction factor of the pier spacing for maximum pier scour depth
K_w	Correction factor of water depth for maximum abutment or pier scour depth
L'	Length of embankment projected normal to flow
L'_{left}	Length of left bridge embankment
L'_{right}	Length of right bridge embankment
L_1	Width of channel in the approach section
L_2	Width of channel in the bridge section
L_f	Width of floodplain
L_t	Design life of a structure
μ_Q	Mean of the normal distribution of daily discharge
μ_y	Mean of the Lognormal distribution of daily discharge
n	Manning's coefficient
ν	Kinematic viscosity of water (10^{-6} m^2/s at 20 ℃)
θ	Attack angle
$\underline{P}$	Probability of exceedance
q_1	Unit discharge at approach section ($=V_1y_1$)
q_2	Unit discharge around abutment ($=V_1y_1A_1/A_2$)
Q_{block}	Discharge blocked by bridge embankment defined by approach average velocity on flood-plain times the area extending the bridge to approach section
Q	Total discharge
Q_{fp1}	Discharge on the floodplain in the approach section immediately upstream of the abutment
ρ	Unit mass of water
R_h	Hydraulic radius
Re	Reynolds number based on pier width (a) or Top width of the abutment (W_a)
Re_{f2}	Reynolds number based on y_{f1} and V_{f2}
S	Spacing between two pier (measured center to center)
Sh	Shape of the pier nose
σ_Q	Standard deviation of the normal distribution of daily discharge
σ_y	Standard deviation of the Lognormal distribution of daily discharge
T_r	Return period
t	Elapsed time after start of scour
t_e	Equivalent time necessary to create the same scour depth as the previous step of discharge
τ_c	Critical shear stress
$\tau_{max(Abut)}$	Maximum shear stress of around abutment
$\tau_{max(Cont)}$	Maximum shear stress of in the middle of channel
$\tau_{max(Pier)}$	Maximum shear stress of around pier
V_1	Mean velocity at the location of the pier if the pier was not there
V_c	Critical velocity of the soil
V_{f1}	Approach average velocity on the floodplain
V_{f2}	Local velocity around the abutment
V_{fc}	Critical velocity on the floodplain
V_{2_HEC}	Velocity in the main channel at the bridge section by HEC-RAS calculation
V_{mc}	Critical velocity in the main channel
W_a	Top width of the abutment or contraction length
y_1	Approach water depth
y_{f1}	Water depth at the toe of the abutment estimated as the water depth immediately upstream of the toe of the abutment
y_{m1}	Water depth in the main channel at immediately upstream of bridge contraction
$y_{s(Abut)}$	Maximum abutment scour depth adjacent to the toe of the abutment
$y_{s(Cont)}$	Maximum contraction scour depth
$y_{s(Pier)}$	Maximum pier scour depth
$y_s(t)$	Scour depth at time t
$\dot{z}$	Erosion rate
$\dot{z}_i$	Initial erosion rate